

REPORT



## Enabling adoption of 2D-NMR for the higher order structure assessment of monoclonal antibody therapeutics

Robert G. Brinson<sup>a</sup>, John P. Marino<sup>a</sup>, Frank Delaglio<sup>a</sup>, Luke W. Arbogast<sup>ib,a</sup>, Ryan M. Evans<sup>b</sup>, Anthony Kearsley<sup>b</sup>, Geneviève Gingras<sup>c</sup>, Houman Ghasriani<sup>ib,c</sup>, Yves Aubin<sup>ib,c</sup>, Gregory K. Pierens<sup>d</sup>, Xinying Jia<sup>ib,d</sup>, Mehdi Mobli<sup>ib,d</sup>, Hamish G. Grant<sup>e</sup>, David W. Keizer<sup>e</sup>, Kristian Schweimer<sup>f</sup>, Jonas Ståhle<sup>ib,g</sup>, Göran Widmalm<sup>g</sup>, Edward R. Zartler<sup>h</sup>, Chad W. Lawrence<sup>i</sup>, Patrick N. Reardon<sup>ib,ti</sup>, John R. Cort<sup>ib,j</sup>, Ping Xu<sup>j</sup>, Feng Ni<sup>j</sup>, Saeko Yanaka<sup>k</sup>, Koichi Kato<sup>k</sup>, Stuart R. Parnham<sup>ib,l</sup>, Desiree Tsao<sup>m</sup>, Andreas Blomgren<sup>ib,n</sup>, Torgny Rundlöf<sup>ib,n</sup>, Nils Trieloff<sup>ib,o</sup>, Peter Schmieder<sup>o</sup>, Alfred Ross<sup>p</sup>, Ken Skidmore<sup>q</sup>, Kang Chen<sup>ib,r</sup>, David Keire<sup>ib,r</sup>, Darón I. Freedberg<sup>ib,s</sup>, Thea Suter-Stahel<sup>t</sup>, Gerhard Wider<sup>t</sup>, Gregor Ilc<sup>u,v</sup>, Janez Plavec<sup>ib,u,v</sup>, Scott A. Bradley<sup>w</sup>, Donna M. Baldisseri<sup>x</sup>, Mauricio Luis Sforça<sup>y</sup>, Ana Carolina de Mattos Zeriz<sup>z</sup>, Julie Yu Wei<sup>aa</sup>, Christina M. Szabo<sup>ib,bb</sup>, Carlos A. Amezcua<sup>ib,bb</sup>, John B. Jordan<sup>cc</sup>, and Mats Wikström<sup>dd</sup>

<sup>a</sup>Institute of Bioscience and Biotechnology Research, National Institute of Standards and Technology and the University of Maryland, Rockville, MD, USA; <sup>b</sup>Applied and Computational Mathematics Division, National Institute of Standards and Technology, Gaithersburg, MD, USA; <sup>c</sup>Centre for Biologics Evaluation, Biologics and Genetic Therapies Directorate, Health Canada, Ottawa, ON, Canada; <sup>d</sup>The Centre for Advanced Imaging, The University of Queensland, St Lucia, QLD, Australia; <sup>e</sup>Bio21 Molecular Science & Biotechnology Institute, The University of Melbourne, Victoria, Australia; <sup>f</sup>Lehrstuhl Biopolymere, Universitaet Bayreuth, Bayreuth, Germany; <sup>g</sup>Department of Organic Chemistry, Arrhenius Laboratory, Stockholm University, Stockholm, Sweden; <sup>h</sup>Analytical R&D, Pfizer Essential Health, Lake Forest, IL, USA; <sup>i</sup>Pacific Northwest National Laboratory, Earth and Biological Sciences Directorate, Richland, DC, USA; <sup>j</sup>Department of Downstream Processing and Analytics, Human Health Therapeutics Research Centre, National Research Council of Canada, Montreal, Quebec, Canada; <sup>k</sup>Institute for Molecular Science and Exploratory Research Center on Life and Living Systems, National Institutes of Natural Sciences, Myodaiji, Okazaki, Japan; <sup>l</sup>Department of Biochemistry and Molecular Biology, Medical University of South Carolina, Charleston, SC, USA; <sup>m</sup>Analytical Development, Momenta Pharmaceuticals, Cambridge, MA, USA; <sup>n</sup>Laboratory Unit, Swedish Medical Products Agency, Laboratory, Uppsala, Sweden; <sup>o</sup>NMR-supported Structural Biology, Leibniz-Forschungsinstitut für Molekulare Pharmakologie (FMP), Berlin, Germany; <sup>p</sup>Roche Pharmaceutical Research & Early Development, Pre-Clinical CMC, Roche Innovation Center Basel, Basel, Switzerland; <sup>q</sup>Analytical Operations, Genentech, South San Francisco, CA, USA; <sup>r</sup>Center for Drug Evaluation and Research, Food and Drug Administration, Maryland, USA; <sup>s</sup>Center for Biologics Evaluation and Research, Food and Drug Administration, Maryland, USA; <sup>t</sup>Department of Biology, Institute of Molecular Biology and Biophysics, ETH Zurich, Zurich, Switzerland; <sup>u</sup>NMR Centre, EN-FIST Centre of Excellence, Ljubljana, Slovenia; <sup>v</sup>NMR Centre, National Institute of Chemistry, Ljubljana, Slovenia; <sup>w</sup>Eli Lilly and Company, Lilly Corporate Center, Indianapolis, IN, USA; <sup>x</sup>MRS – Application Science, Bruker BioSpin Corporation, Billerica, MA, USA; <sup>y</sup>Brazilian Biosciences National Laboratory (LNBio), Brazilian Center for Research in Energy and Materials (CNPEM), Campinas, Brazil; <sup>z</sup>Brazilian Synchrotron Light Laboratory (LNLS), Brazilian Center for Research in Energy and Materials (CNPEM), Campinas, Brazil, CEP; <sup>aa</sup>Protein Product Development, Biogen Inc., Cambridge, MA, USA; <sup>bb</sup>Baxter Pharmaceuticals R&D, Baxter Healthcare, Round Lake, IL, USA; <sup>cc</sup>Global Regulatory and R&D Policy, Amgen Inc., Thousand Oaks, CA, USA; <sup>dd</sup>Higher Order Structure, Attribute Sciences, Amgen Inc., Thousand Oaks, CA, USA

### ABSTRACT

The increased interest in using monoclonal antibodies (mAbs) as a platform for biopharmaceuticals has led to the need for new analytical techniques that can precisely assess physicochemical properties of these large and very complex drugs for the purpose of correctly identifying quality attributes (QA). One QA, higher order structure (HOS), is unique to biopharmaceuticals and essential for establishing consistency in biopharmaceutical manufacturing, detecting process-related variations from manufacturing changes and establishing comparability between biologic products. To address this measurement challenge, two-dimensional nuclear magnetic resonance spectroscopy (2D-NMR) methods were introduced that allow for the precise atomic-level comparison of the HOS between two proteins, including mAbs. Here, an inter-laboratory comparison involving 26 industrial, government and academic laboratories worldwide was performed as a benchmark using the NISTmAb, from the National Institute of Standards and Technology (NIST), to facilitate the translation of the 2D-NMR method into routine use for biopharmaceutical product development. Two-dimensional <sup>1</sup>H,<sup>15</sup>N and <sup>1</sup>H,<sup>13</sup>C NMR spectra were acquired with harmonized experimental protocols on the unlabeled Fab domain and a uniformly enriched-<sup>15</sup>N, 20%-<sup>13</sup>C-enriched system suitability sample derived from the NISTmAb. Chemometric analyses from over 400 spectral maps acquired on 39 different NMR spectrometers ranging from 500 MHz to 900 MHz demonstrate spectral fingerprints that are fit-for-purpose for the assessment of HOS. The 2D-NMR method is shown to provide the measurement reliability needed to move the technique from an emerging technology to a harmonized, routine measurement that can be generally applied with great confidence to high precision assessments of the HOS of mAb-based biotherapeutics.

### ARTICLE HISTORY

Received 12 July 2018  
Revised 18 October 2018  
Accepted 31 October 2018


### KEYWORDS

monoclonal antibody (mAb) therapeutics; NISTmAb; higher order structure; nuclear magnetic resonance spectroscopy (NMR); comparability; chemometrics

**CONTACT** Robert G. Brinson  [robert.brinson@nist.gov](mailto:robert.brinson@nist.gov)

<sup>†</sup>Present address: Oregon State University, Corvallis, Oregon 97331, United States

Color versions of one or more of the figures in the article can be found online at [www.tandfonline.com/kmab](http://www.tandfonline.com/kmab).

 Supplementary material can be accessed [here](#)

© 2018 The Author(s). Published with license by Taylor & Francis Group, LLC

This is an Open Access article distributed under the terms of the Creative Commons Attribution-NonCommercial-NoDerivatives License (<http://creativecommons.org/licenses/by-nc-nd/4.0/>), which permits non-commercial re-use, distribution, and reproduction in any medium, provided the original work is properly cited, and is not altered, transformed, or built upon in any way.

## Introduction

Prescription drug revenue from biotechnology products accounted for approximately US\$153 billion in 2017 for the top ten drug companies.<sup>1</sup> Of the top 10 biologic drugs in 2017, 6 were from the monoclonal antibody therapeutic class.<sup>2</sup> Indeed, mAb-based molecules are currently the dominant biotherapeutic platform, including over 50 that are in late-stage clinical studies.<sup>3</sup> The development and adoption of new technologies have been encouraged by regulatory agencies,<sup>4</sup> and have become indispensable for the characterization of the quality attributes (QA) that may affect the safety and efficacy of these large and complex drugs. One attribute that is unique to biologics, including mAbs, is known as higher order structure (HOS), which is composed of the secondary, tertiary, and quaternary structure.<sup>5</sup> The HOS of a protein is a QA that is directly linked to the function of the molecule, and is therefore a key determinant in assessing structural similarity between different manufactured drug lots and between a biosimilar and an originator molecule in biosimilarity evaluations. The measurement of the HOS of a protein therapeutic represents a substantial analytical challenge. Unlike small molecule drugs that are chemically derived and for which structure can be determined absolutely, the HOS of protein therapeutics precludes absolute characterization due to the large molecular weight, protein dynamics, and product heterogeneity arising from subtle differences in the manufacturing process.<sup>5–8</sup>

To date, the evaluation of HOS for protein therapeutic quality control purposes in the pharmaceutical industry has generally been carried out using methods with low-to-moderate structural resolution such as circular dichroism (CD), Raman, or Fourier transform infrared (FT-IR) spectroscopies, as well as indirect techniques that measure structure as it relates to thermal stability or biological function.<sup>9</sup> Recently, the application of two-dimensional (2D) heteronuclear  $^1\text{H}$ , $^{15}\text{N}$ - or  $^1\text{H}$ , $^{13}\text{C}$ -correlated NMR spectra to characterize the HOS of protein therapeutics has garnered great interest in the biopharmaceutical community because a single 2D-NMR experiment can yield a spectral map that offers a comprehensive, atomic-level fingerprint of the primary, secondary, tertiary and quaternary structure(s) of a protein therapeutic.<sup>8,10–12</sup> Indeed, a correctly folded protein molecule typically affords a defined pattern of cross-peaks resulting from individual  $^1\text{H}$ , $^{15}\text{N}$  amide or  $^1\text{H}$ , $^{13}\text{C}$  methyl resonance correlations, referred to as the “2D spectral fingerprint.” These signals are observed at specific frequency positions that relate to the unique chemical and structural environments of those individual atoms in the three-dimensional protein structure,<sup>13,14</sup> assuming experimental sample conditions, such as temperature, pH, and ionic strength, are properly controlled. Deviations in the sample conditions of a protein may affect the electronic environment of the nuclei, and therefore may perturb the chemical shift positions. Such effects can be utilized with great benefit to judge the spectral response for any given sample, and to extract detailed protein structural information, such as the

mapping of several perturbed signals to loop regions from a temperature deviation<sup>15</sup> or the elucidation of excipient interactions to specific residues with the target protein.<sup>16,17</sup> However, for the purpose of structural assessment of therapeutic proteins by NMR under controlled sample conditions, the precise matching of two 2D-NMR spectral fingerprints of a protein from two products provides a high level of assurance that the predominant structure(s) of the proteins is highly similar between those two product samples. Such a determination of “high similarity” could aid in the designation of analytical similarity between the two products in combination with other relevant QAs.<sup>18</sup>

Originally applied to relatively small recombinant protein therapeutics (< 25 kDa) at natural isotopic abundance,<sup>10</sup> the capability of the 2D-NMR approach to provide high resolution HOS data has more recently been demonstrated for the mAb therapeutic class (~ 150 kDa).<sup>11,19–21</sup> For example, as applied to mAbs, measurement of a  $^1\text{H}$ , $^{13}\text{C}$  methyl fingerprint was found to afford advantages over the  $^1\text{H}$ , $^{15}\text{N}$  amide-based NMR fingerprint, owing to the greater natural abundance of  $^{13}\text{C}$  relative to  $^{15}\text{N}$  (1.1% versus 0.37%) and the more advantageous relaxation behavior of the freely rotating methyl moieties compared to amide groups.<sup>19</sup> Indeed, acquisition of  $^1\text{H}$ , $^{13}\text{C}$  NMR spectra on an intact mAb using an ultra-high field NMR spectrometer was shown to be practical. In these studies, the intact mAb was also cleaved with papain into component parts, and the 2D-NMR method was applied to the resulting antigen-binding fragment (Fab) and the crystallizable fragment (Fc), confirming that higher order structural information of the fragments was retained when compared to the intact mAb molecule.

Here, we report a comprehensive inter-laboratory study that establishes benchmarks for the adoption of the 2D-NMR methods for robust precision measurement of mAb HOS. The study, conducted by 26 laboratories with roughly equal representation from industry, academia and government, recorded a total of 451 2D-NMR spectra using the unlabeled NIST-Fab, derived from the NISTmAb Primary Sample (PS) #8670, and a uniformly enriched (U)- $^{15}\text{N}$ , 20% enriched- $^{13}\text{C}$  NIST-Fab expressed in *P. pastoris* that served as the system suitability sample (SSS). The NISTmAb is a publicly available reference material intended for evaluating analytical techniques applied to mAb therapeutics,<sup>22–24</sup> and the Fab domain from the NISTmAb was chosen as the target of this study to ensure that the measurements would be amenable to the moderate field NMR spectrometers employed by some laboratories in this report (e.g., 500 MHz to 700 MHz). Using weighted peak lists from both  $^1\text{H}$ , $^{15}\text{N}$  amide, and  $^1\text{H}$ , $^{13}\text{C}$  methyl spectra, chemometric methods demonstrate that reliable spectral fingerprints can be generated using NMR spectrometers with magnetic fields ranging from 500 MHz to 900 MHz, of different vintages of vendor instrumentation and equipped with conventional or high sensitivity NMR probes. The results provide confidence that the 2D-NMR method is reliable for routine application in biopharmaceutical development and suitable for regulatory purposes.

## Results

### Visual inspection of 2D $^1\text{H}$ , $^{15}\text{N}$ and $^1\text{H}$ , $^{13}\text{C}$ spectral fingerprints

The NIST-Fab, derived from papain digestion of the NISTmAb PS #8670, was chosen as the test material for this study, since this domain should be a representative of the IgG1 $\kappa$  mAb therapeutic class. While the HOS of intact mAbs can be characterized using 2D-NMR at natural isotopic abundance,<sup>25</sup> previous work has also established that the 2D-NMR spectral map of an Fc or Fab retains much of the HOS information relevant to the intact mAb.<sup>19</sup> This work showed that all but a few methyl resonances were unchanged in the fragments relative to the intact mAb. Since there are several methyl-bearing residues around the hinge region, the small number of chemical shift perturbations from papain cleavage points to a local change in the electronic environment and supports the conclusion that the overall global structure of the fragments is maintained. Taken together with the fact that an isotopically enriched SSS of the NIST-Fab could be generated using a *P. pastoris* expression system, the NIST-Fab provided a good model system for benchmarking the 2D-NMR method for application to mAbs. Both the SSS and the NIST-Fab were distributed to all laboratories from the same sample batches. Various 2D-NMR methods, summarized in Table 1, were then applied to both samples. Each method type was given an experimental code (e.g., D1A, E1B, etc.). All partnering laboratories were asked to perform the D-type experiments and additionally had the option of collecting spectra with different parameters or pulse sequences (E-type experiments). Data from each institution were anonymized by a third party (see Materials and Methods), and each laboratory was assigned a 4-digit institutional identifier followed by a 3-digit experiment number, yielding a complete experimental code of 10 characters (e.g., D2A-1247-001). The total breakdown of collected spectra per institution and experimental type is given in Table S1.

The SSS used in the study was uniformly enriched in  $^{15}\text{N}$  and 20%-enriched in  $^{13}\text{C}$  (U- $^{15}\text{N}$ , 20%- $^{13}\text{C}$  NIST-Fab). The signal peptide on the SSS was not fully cleaved during expression, affording a molecule with eight extra amino acids, four each on the N-termini of the light and heavy chains, relative to the NIST-Fab. This sequence difference was fortuitous, however, as the SSS and the NIST-Fab provided a sample set of two structurally similar but not identical molecules that could be used to test the performance of different chemometric methods. From a visual inspection of the NIST-Fab and SSS 2D  $^1\text{H}$ ,  $^{15}\text{N}$  amide and  $^1\text{H}$ ,  $^{13}\text{C}$  methyl spectra, these 2D spectral fingerprints suggest that the molecules are structurally similar, with almost all cross peaks overlapping due to the high sequence and structural identity between the two molecules (Figures 1 and 2). A few shifted cross peaks were observed, as would be expected due to the structural differences arising from the extended amino acid sequence at the N-termini of both the heavy and light chains of the SSS relative to the NIST-Fab.

The 'gold standard' for the evaluation of a protein's folded state by NMR is the 2D  $^1\text{H}$ ,  $^{15}\text{N}$  NMR spectral map that provides a single-bond correlation for every NMR-observable non-proline backbone amide and a number of amino acid side chains (e.g., asparagine, arginine, and glutamine) (Figure 1). For the SSS, these spectra were acquired with moderate (500 MHz) to very high (900 MHz) quality, spectral resolution and sensitivity, allowing this study to be benchmarked against previous work.<sup>15</sup> However, the collection of the  $^1\text{H}$ ,  $^{15}\text{N}$  spectral map at natural isotopic abundance for the unlabeled NIST-Fab at lower fields (500 MHz – 700 MHz) was considered impractical for the benchmarking exercise due to insufficient sensitivity of these experiments at the lower magnetic fields, and was therefore not attempted. At 900 MHz, a high quality spectrum was recorded to allow visual comparison of this standard spectral map between the NIST-Fab and SSS (Figure 1b, c and d). This experiment required a total acquisition time of 69 h, even with the use of acquisition techniques designed to shorten overall

**Table 1.** Summary of required and optional 2D-NMR experiments. See Tables S5 – S9 for detailed experimental parameters.

Experiment Code	Number of Spectra	Type of Experiment	Sample	Sampling Type	Comments
<b>Required Experiments</b>					
D1A	30	$^1\text{H}$ , $^{15}\text{N}$ gHSQC <sup>1</sup>	SSS <sup>2</sup>	US <sup>3</sup>	Field dependent acquisition:20 ms in $t_1$
D2A	39	$^1\text{H}$ , $^{13}\text{C}$ gHSQC	SSS	US	Field independent acquisition:128 total points in $t_1$
D2B	32	$^1\text{H}$ , $^{13}\text{C}$ gHSQC	SSS	NUS <sup>4</sup>	50% NUS of D2A
D2C	41	$^1\text{H}$ , $^{13}\text{C}$ gHSQC	SSS	US	Field dependent acquisition:25 ms in $t_1$
D2D	31	$^1\text{H}$ , $^{13}\text{C}$ gHSQC	SSS	NUS	50% NUS of D2C
D2E	26	$^1\text{H}$ , $^{13}\text{C}$ gHSQC	SSS	NUS	Twice the scans per increment, 50% NUS of D2C
D3A	47	$^1\text{H}$ , $^{13}\text{C}$ gHSQC	NIST-Fab	US	Field dependent acquisition:25 ms in $t_1$
D3B	36	$^1\text{H}$ , $^{13}\text{C}$ gHSQC	NIST-Fab	NUS	50% NUS of D3A
<b>Optional Experiments</b>					
E1	7	$^1\text{H}$ , $^{13}\text{C}$ gHSQC	NIST-Fab	Either	One parameter change from required experiments
E1A	45	$^1\text{H}$ , $^{13}\text{C}$ gHSQC	Either	NUS	Customized sampling schedule generated by individual laboratory
E1B	48	$^1\text{H}$ , $^{13}\text{C}$ gHSQC	Either	Either	Different temperatures:15 °C, 25 °C, 45 °C, or 50 °C
E1C	23	$^1\text{H}$ , $^{13}\text{C}$ sfHMQC <sup>5</sup>	Either	Either	sfHMQC pulse sequence
E2	11	$^1\text{H}$ , $^{15}\text{N}$ gHSQC	Either	US	One parameter change from D1A
E2N	2	$^1\text{H}$ , $^{15}\text{N}$ gHSQC	SSS	NUS	Customized NUS schedule generated by individual laboratory
E2A	14	$^1\text{H}$ , $^{15}\text{N}$ gHSQC	SSS	US	Different temperatures:15 °C, 25 °C, 45 °C, or 50 °C
E2B	8	$^1\text{H}$ , $^{15}\text{N}$ pHSQC	Either	US	Phase sensitive HSQC pulse sequence
E2C	11	$^1\text{H}$ , $^{15}\text{N}$ sfHMQC	Either	Either	SOFAS-HMQC pulse sequence

<sup>1</sup>gHSQC = gradient selected heteronuclear single quantum coherence spectroscopy

<sup>2</sup>SSS = system suitability sample

<sup>3</sup>US = uniform sampling

<sup>4</sup>NUS = non-uniform sampling

<sup>5</sup>sfHMQC = selective optimized flip angle short transient (SOFAS) heteronuclear multiple quantum coherence spectroscopy (HMQC)



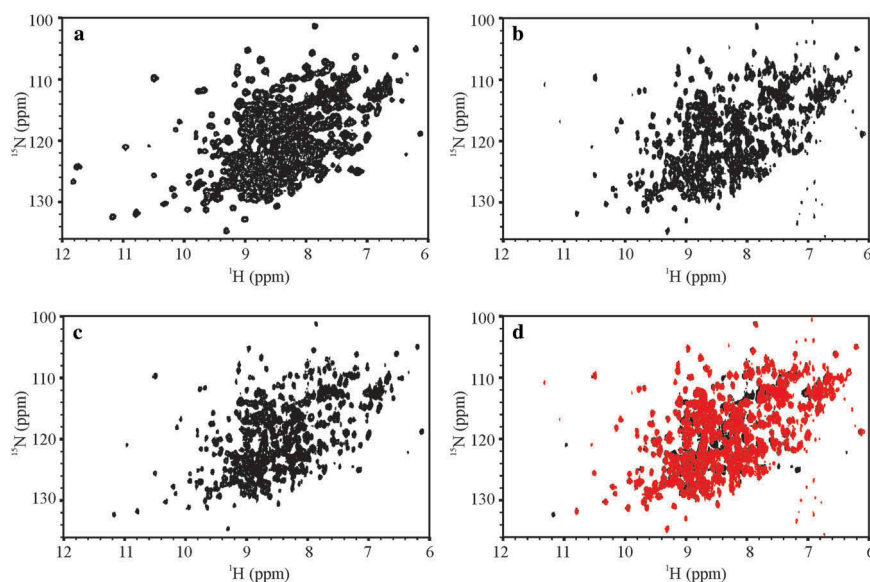


**Figure 1.** Representative 500 MHz and 900 MHz  $^1\text{H}$ ,  $^{15}\text{N}$  spectral fingerprints of the SSS and the NIST-Fab. (a)  $^1\text{H}$ ,  $^{15}\text{N}$  gHSQC D1A-3897-009 spectrum of the SSS recorded with uniform sampling at 500 MHz; (b)  $^1\text{H}$ ,  $^{15}\text{N}$  SOFAST-HMQC E2C-8822-030 spectrum of the NIST-Fab using 50% NUS at 900 MHz; (c)  $^1\text{H}$ ,  $^{15}\text{N}$  gHSQC E2N-8822-071 spectrum of the SSS using 50% NUS at 900 MHz; (d) Spectral overlay of the NIST-Fab, in red, of E2C-8822-030 with the SSS, in black, of E2N-8822-071 at 900 MHz. A  $^1\text{H}$ ,  $^{15}\text{N}$  spectral fingerprint was not measured for the NIST-Fab at 500 MHz because the  $^1\text{H}$ ,  $^{15}\text{N}$  gHSQC was too insensitive to measure the spectral map for the NIST-Fab at  $^{15}\text{N}$  natural isotopic abundance. All representative spectra were collected at 37 °C and are plotted just above the noise threshold. The extra peaks at 500 MHz between  $\delta_{\text{H}}$  11 ppm – 12 ppm are field dependent resonances whose intensity slowly decreases due to dynamics on the NMR time scale as the magnetic field increases from 500 MHz to 900 MHz; the frequencies of these field dependent resonances are the same regardless of the magnetic field. In spectrum E2C-8822-030, the observed vertical artifacts around 7 ppm arose from high amplitude noise that is intrinsic to the SOFAST-HMQC experiment. For a summary of experimental codes, see Table 1.

experimental times, *i.e.*, selective optimized flip angle short transient (SOFAST) pulsing<sup>26</sup> and 50% non-uniform sampling (NUS).<sup>27</sup> As a result of the limitations in acquiring  $^1\text{H}$ ,  $^{15}\text{N}$  spectral data for the NIST-Fab, the peak list for assessing inter-laboratory variability was generated using only spectra collected on the SSS at 37 °C (Figure S1). The lowest resolution spectrum, generated at 500 MHz, was used as the reference to generate the limiting peak list, which gave 34% of the total expected peaks due to the high degree of spectral overlap. This reference peak list was then copied to all other  $^1\text{H}$ ,  $^{15}\text{N}$  spectra recorded at 37 °C.

In contrast to the  $^1\text{H}$ ,  $^{15}\text{N}$  2D-NMR spectra, the  $^1\text{H}$ ,  $^{13}\text{C}$  spectral map of the methyl region provided at least a 10-fold faster approach for 2D-NMR spectral comparison of the HOS of the SSS and the NIST-Fab due to the higher natural abundance of  $^{13}\text{C}$  compared to  $^{15}\text{N}$  and intrinsically more favorable relaxation of methyl groups due to free rotation of the methyl protons about the carbon-carbon bond axis (Figure 2). Indeed, high quality spectra for the NIST-Fab could be measured at the lowest field used in this study (*i.e.*, 500 MHz) in as little as 7 h with the application of 50% NUS. Using the lowest resolution spectra, which were recorded at 500 MHz as the threshold spectra for peak picking for the full spectral dataset, a peak list with approximately 41% of the expected cross peaks could be defined due to the high degree of spectral overlap (Figures S2 and S3). This peak list was subsequently overlaid on all other  $^1\text{H}$ ,  $^{13}\text{C}$  spectra acquired in the study to allow further in-depth comparative analysis of the spectra.

### Combined chemical shift deviation as a metric for spectral comparability and determination of inter-laboratory precision

Combined chemical shift deviation (CCSD)<sup>28</sup> was used to demonstrate the high precision of the 2D-NMR measurement for spectra recorded at 37 °C. A previous study reported a precision of better than 8 ppb for  $^1\text{H}$ ,  $^{15}\text{N}$  CCSD for filgrastim samples.<sup>15</sup> From the CCSD analysis of 41 uniformly sampled  $^1\text{H}$ ,  $^{15}\text{N}$  spectral maps in the current study recorded for the SSS at 37 °C, a very high precision ( $3.3 \pm 1.8$  ppb) was determined (Figure 3a). Since this use of CCSD evaluates the precision of the mean deviation of a given chemical shift, the 95% confidence intervals are reported as standard error of the mean (SEM).

The availability of the much larger set of  $^1\text{H}$ ,  $^{13}\text{C}$  spectra collected in this study further allowed for a greater in-depth CCSD precision analysis than available from the previous work.<sup>15</sup> As expected, the precision was slightly higher for this data relative to the  $^1\text{H}$ ,  $^{15}\text{N}$  spectra, with an average CCSD of  $2.8 \pm 0.5$  ppb, for the benchmark D2A and D2C  $^1\text{H}$ ,  $^{13}\text{C}$  spectra (Figure 3b and Figure S4). Indeed, the precision remained high, and the 95% confidence intervals were tight for all variations of data acquisition. The higher S/N ratio also afforded slightly greater precision for D2E class experiments ( $2.3 \pm 0.8$  ppb), which were recorded with double the number of scans per  $^{13}\text{C}$  increment compared to all other D2-type spectra (Table 1). Only spectra acquired with custom NUS schedules and the SOFAST-HMQC (heteronuclear multiple quantum coherence) pulse sequence had slightly less

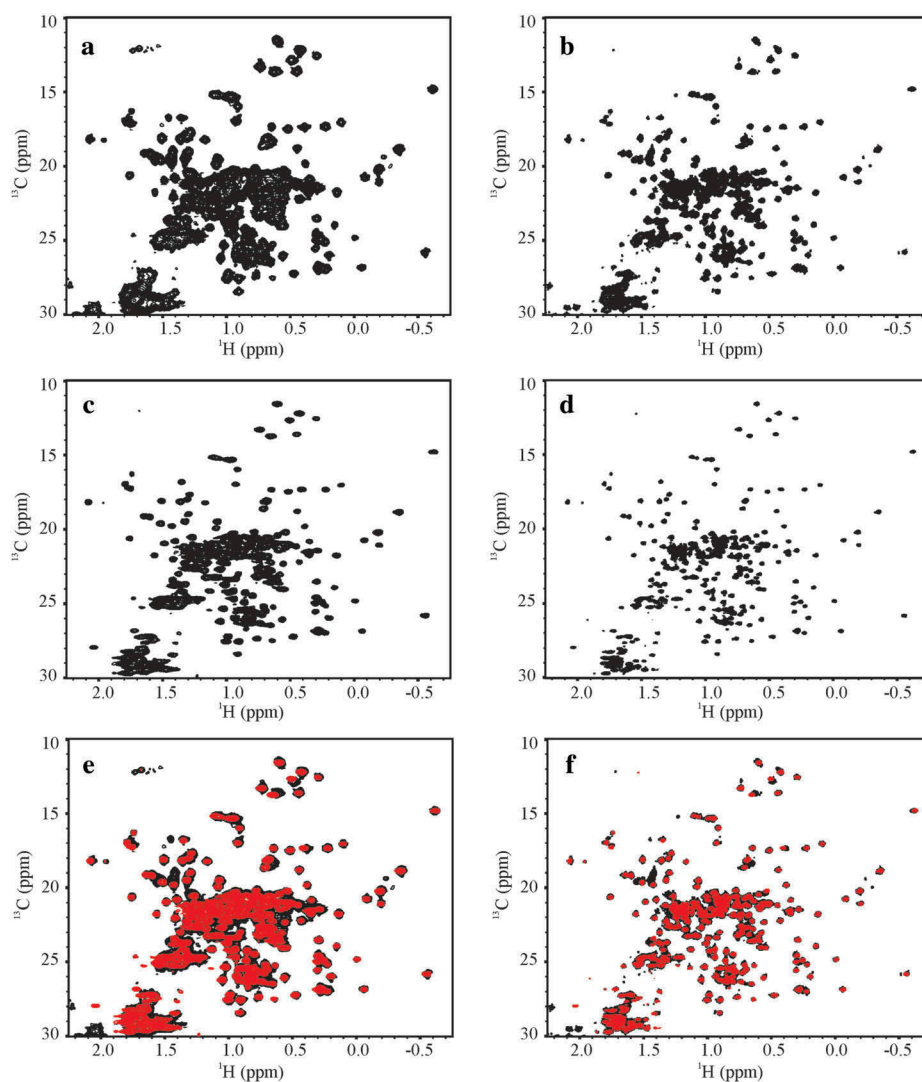


**Figure 2.** Representative  $^1\text{H}$ ,  $^{13}\text{C}$  gHSQC spectral fingerprints of the SSS and the NIST-Fab. (a) D2C-3897–012 spectrum of SSS at 500 MHz and (b) D2C-7425–012 spectrum of SSS at 900 MHz; (c) D3A-3897–015 spectrum of the NIST-Fab at 500 MHz and (d) D3A-7425–015 spectrum of the NIST-Fab at 900 MHz; and overlay of SSS, in black, and the NIST-Fab, in red, at (e) 500 MHz and (f) 900 MHz. All representative spectra were collected at 37 °C. For a summary of experimental codes, see Table 1.

precision of  $5.3 \pm 2.7$  ppb and  $5.3 \pm 2.8$  ppb, respectively. Overall, the exquisite reproducibility of frequency positions of the spectral cross peaks observed in the 2D-NMR experiments is quantitatively demonstrated by these average CCSD values.

### Principal component analysis of $^1\text{H}$ , $^{13}\text{C}$ spectra

Principal component analysis (PCA) of  $^1\text{H}$ ,  $^{13}\text{C}$  weighted peak lists from all spectra afforded distinct groups that could be manually clustered according to sample type and reported temperature of the sample during spectral acquisition (Figure 4a). The PCA confirms that the spectral map is highly reproducible regardless of the acquisition method used across the 26 laboratories, with the few outliers readily explained by experimental set-up, including choice of NUS schedule (Figures S5 and S6) and sample temperature deviation (Figures S7 and S8, Table S2). When PCA was re-applied to only spectra measured at 37 °C, for which the largest sample size is available ( $n = 307$ , Figure S9), then the known systematic pulse program error in the

acquisition of a subset of spectra from older hardware became apparent (Figure S10). However, as illustrated by the analyses of the few outliers, proper experimental set-up and proper sample controls (e.g., temperature, pH, ionic strength, and concentration) are crucial for optimal spectral reproducibility.

Several chemometric clustering algorithms were also applied to the PCA plot of peak tables for all  $^1\text{H}$ ,  $^{13}\text{C}$  spectra, including  $k$ -means (*analysis not shown*),  $k$ -medoids (Figure S11), min-max group pair algorithm (Figure S12), and unweighted pair group method with arithmetic mean (UPGMA, Figure 4b and Figure S13). The  $k$ -means and  $k$ -medoids algorithms performed particularly poorly; this was likely due, in part, to the fewer number of spectra collected at different temperatures (see Table 1, experimental type: E1B). The min-max group pair clustering method performed better, although this approach classified the SSS 45 °C and SSS 50 °C spectra as one group when seven clusters were specified (Figure S12). However, both the min-max group pair and the UPGMA algorithms correctly identified clusters when eight clusters were specified, including

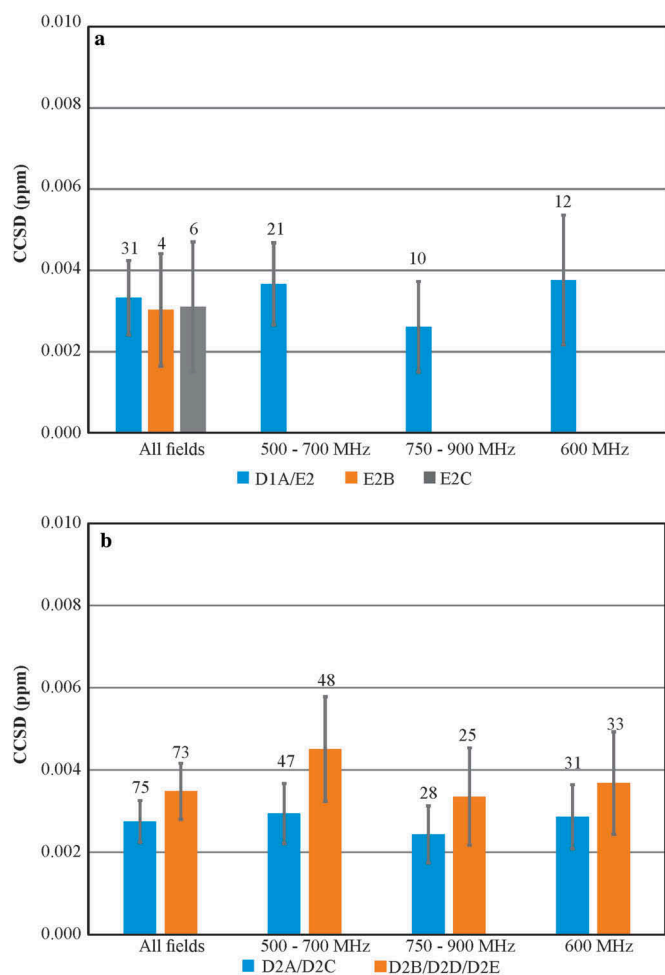


**Figure 3.** Average Combined Chemical Shift Deviation (CCSD) precision plots of required experiments at 37 °C. **(a)** CCSD of  $^1\text{H}$ ,  $^{15}\text{N}$  D1A/E2, E2B, and E2C spectra; **(b)** CCSD of D2A/D2C and D2B/D2D/D2E  $^1\text{H}$ ,  $^{13}\text{C}$  spectra. All  $^1\text{H}$ ,  $^{15}\text{N}$  spectra and  $^1\text{H}$ ,  $^{13}\text{C}$  D2A/D2C spectra were acquired with uniform sampling, while  $^1\text{H}$ ,  $^{13}\text{C}$  D2B/D2D/D2E spectra were 50% non-uniformly sampled. The number above each bar represents the total number of spectra included in the analysis for each respective experimental type. For  $^1\text{H}$ ,  $^{15}\text{N}$  CCSD plot, E2 experiments were included since the only parameter change from D1A was a smaller  $^{15}\text{N}$  spectral width. Errors bars represent 95% confidence intervals of SEM. For detailed breakdown of experimental codes, see **Table S10**.

the assignment of the temperature outlier D2E-8822-065 to the 45 °C SSS cluster (**Figure 4b**, **S7** and **S8**).

## Discussion

HOS assessment is critical in determining the comparability of the drug substance over the course of manufacturing changes that may occur through the lifecycle of a protein therapeutic.<sup>29</sup> This assessment is also a key piece of information in biosimilarity evaluations that use comparative analysis of the physico-chemical properties of a biosimilar to its reference product. Assurances that the primary, secondary, and higher order structures of two proteins are highly similar is generally considered to be a strong indication of similar function. Therefore, the ability to precisely and accurately compare structural attributes of two proteins (*e.g.*, a biosimilar and its reference product) with the atomic resolution afforded by NMR can provide key information on the degree of structural similarity, thereby contributing to the totality of the evidence and supporting a more targeted and selected approach to clinical studies for the confirmation of the safety and efficacy of the proposed biosimilar.<sup>4,18,30</sup>

Of all the HOS techniques, 2D-NMR is the only analytical method that can simultaneously yield precise and accurate information about the primary, secondary, tertiary, and quaternary (*i.e.*, HOS) structure of a biopharmaceutical in solution with atomic level resolution. Analysis of NMR spectral peak positions has many beneficial attributes for assessing HOS. Even in the absence of sequence specific resonance assignments, each cross peak represents a reporter of the local structural environment at atomic resolution that is exquisitely sensitive to its magnetic (*e.g.*, chemical and structural) environment. Since the chemical shift is a fundamental property of each NMR-active nucleus in a molecule, the position (in ppm) relative to a standard reference compound is a truly robust HOS parameter, since it can be measured with high accuracy and precision regardless of spectrometer magnetic field, choice of pulse sequence, or acquisition sampling strategy, provided that experimental sample conditions

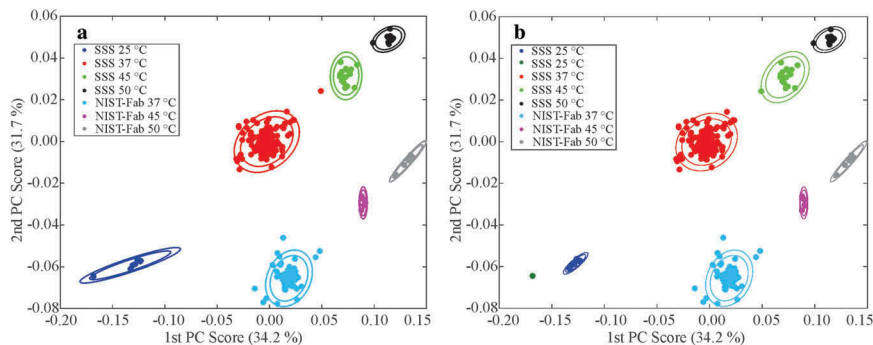


**Figure 4.** Clustered PCA scatter plots of all peak lists from 354  $^1\text{H}$ ,  $^{13}\text{C}$  spectra. **(a)** Manually clustered plot according to reported sample-type and temperature. The centroid of each manual cluster was then determined. **(b)** Clustering output for  $k = 8$  for both the Unweighted Pair Group Method with Arithmetic Mean (UPGMA) and mix-max group pair algorithms. The inner and outer ellipses represent 95% and 99% confidence regions, respectively, based upon chi-square probabilities. In panel **b**, both algorithms afforded the same spectral clusters, so only one plot is shown. See **Figures S12** and **S13** for different data clustering ( $k = 7$  and  $9$ ) for the mix-max group pair and UPGMA algorithms, including a discussion of the chemometric classification of the outliers. For additional details on the outliers, see the main text and **Figures S5 – S10**.

(e.g., temperature, ionic strength, concentration, and pH) are properly controlled. Indeed, any degradation or post-translation modifications will lead to spectral shifts that could be directly attributable to a perturbation in HOS. The extent to which a change in HOS results in chemical shift perturbations in the spectral fingerprint of a biopharmaceutical will depend on the nature of the structural change and will likely be product specific. In one example, 2D-NMR has been shown to detect even the most subtle effects on HOS resulting from engineered NISTmAb glycoform populations via PCA.<sup>25</sup> To aid in the identification of HOS perturbations, further cross peak parameters (e.g., peak volumes or line widths) could additionally be included to parse the structural and dynamic properties of the molecule of interest. Indeed, the inclusion of line widths, which are roughly proportional to molecular weight, could allow the detection of soluble aggregates and the concomitant loss of a monomer population, which is an important metric that could adversely affect the pharmacological activity of a therapeutic.

In terms of data sampling, the generation of a NUS schedule with a well-established algorithm such as Poisson-gap<sup>31</sup> assures comparable high chemical shift precision to uniform sampling. In fact, most apparent outliers in the PCA plots (Figure 4, Figures S5 and S9), with the exception of E1A-5479-103 that was collected with an alternative NUS schedule (Figure S6), still had very precise peak positions as shown by CCSD, highlighting the reproducibility of the 2D-NMR method to define the spectral fingerprint. Moreover, this benchmarking study confirmed that this approach provides quality spectral discrimination of Fab domains even at 500 MHz, the lowest field represented in this study. Further, the chemometric approach using PCA with peak tables provides a means to appropriately and sufficiently cluster mAb product samples by HOS with only approximately 41% of the expected methyl cross peaks from the common peak list of the SSS and the NIST-Fab (see Results section). Nonetheless, for the highest stringency for comparability purposes, the use of the highest available magnetic field is recommended. In fact, using an arbitrary peak list developed only for the NIST-Fab from D3A spectra at 37 °C, up to 91% spectral coverage can be achieved using an ultra-high field magnet, affording even greater assurance that any potentially important spectral changes will be observable (Table S3).

Overall, this multi-national inter-laboratory comparison from industry, academia, and government has established a community standard for the measurement of the HOS QA by the 2D-NMR method at atomic resolution. Since the NIST-Fab is representative of the IgG1 therapeutic class, the dominant mAb platform, we fully expect the conclusions of this study to apply to all other members in this important class, and a recent report applying the 2D-NMR method to six therapeutic mAb-based products suggests that this is indeed the case.<sup>21</sup> This benchmarking exercise therefore provides confidence for the industrial and regulatory agencies that 2D-NMR HOS characterization is a practical method that can be performed both with high repeatability and reproducibility on large protein drugs. The results of the study further demonstrate the rigorous capability of the 2D-NMR method, when

combined with chemometric analysis tools, to determine whether the HOS of comparators (e.g., multiple lot numbers, different formulations,<sup>16,17</sup> or a biosimilar to a reference product) is highly similar. Indeed, we propose that the generated data may serve as a reference database for mAb NMR studies in development, quality control, and post-licensure supervision of the products. Since the NISTmAb has been developed by NIST into a reference material (RM #8671), any laboratory may obtain this molecule, follow the standardized protocol described in this report to record 2D-NMR spectra, and assure system suitability in similarity studies on other prospective products. In addition, based on the method robustness, accuracy, and precision observed in this large study, the potential exists that individual mAb manufacturers may measure the NMR fingerprint on an original clinically tested safe and efficacious product, store these data in a reference library and compare data from future batches by chemometric approaches to the original across the therapeutic lifecycle of the drug. Such high information content comparisons of key attributes like HOS increase the confidence in the drug's quality across manufacturing changes or manufacturing sites. As such, the study moves the 2D-NMR method from an emerging technology to a harmonized, routine measurement that can be generally applied with great confidence to high precision assessments of the HOS of a wide-array of protein therapeutics.

## Material and methods

### Study design

The overall design was to benchmark and to harmonize the 2D-NMR spectral method for the assessment of HOS of large protein biologics and/or domains from these proteins. As a representative molecule of the mAb therapeutic class, the NISTmAb PS #8670 was chosen due to the wealth of publicly available knowledge on the molecule<sup>32</sup> and its development into a reference material (RM # 8671) for the biopharmaceutical industry.<sup>23,24</sup> To make the measurements more practical for moderate field NMR spectrometers, e.g., 500 MHz to 700 MHz, the Fab domain was generated from the NISTmAb PS #8670.<sup>19</sup> To serve as a highly sensitive standard sample to test multiple measurement parameters, an isotopically enriched U-<sup>15</sup>N, 20%-<sup>13</sup>C SSS was produced.

### Production of the system suitability sample

The U-<sup>15</sup>N, 20%-<sup>13</sup>C NIST-Fab, referred to as the SSS, was produced by expression in *Pichia pastoris*. The heavy and light chains, corresponding to the sequence of the Fab domain obtained after papain cleavage of the NISTmAb, were produced using a bicistronic expression vector using the Invitrogen *Pichia Pastoris* Expression kit (Life Technologies, Carlsbad, CA) that secretes the folded protein product into the growth media. Isotope labeling was carried out using <sup>15</sup>N-ammonium sulfate (Sigma Aldrich Corp., St. Louis, MO) as the sole nitrogen source and <sup>13</sup>C-methanol (Cambridge Isotope Laboratories, Tewksbury, MA) as the labeled carbon source. The product was purified using an IgG-CH1 affinity column (ThermoFisher Scientific,



Waltham, MA). Subsequent mass spectral analysis confirmed that the yeast signal peptide was not fully cleaved, leaving an extra tetrapeptide of Glu-Ala-Glu-Ala on the N-termini of both the heavy and light chains. The purified U-<sup>15</sup>N, 20%-<sup>13</sup>C NIST-Fab was buffer exchanged into 25 mM bis-tris-*d*19 (Cambridge Isotope Laboratories, Tewksbury, MA) pH 6.0 in 5% D<sub>2</sub>O and adjusted with the same buffer to the final concentration of 53 μM. All quality control checks were performed on the final, pooled sample. These included polyacrylamide gel electrophoresis (PAGE) and 2D <sup>1</sup>H, <sup>15</sup>N and <sup>1</sup>H, <sup>13</sup>C gradient-selected heteronuclear single quantum coherence spectroscopy (gHSQC) experiments. The PAGE (4% – 12% acrylamide, 200 V, ThermoFisher Scientific, Waltham, MA) was performed with the NuPAGE MES-SDS running buffer (ThermoFisher Scientific, Waltham, MA), which included 2.5 mM 2-(N-morpholino)ethanesulfonic acid, 2.5 mM tris base, 0.05 mM ethylenediaminetetraacetic acid (EDTA), 0.005% sodium dodecyl sulfate (SDS), pH 7.3. For the NMR quality control checks, the 2D spectra were acquired on a 900 MHz Bruker Avance III spectrometer (Billerica, MA) equipped with a triple resonance cryogenically-cooled TCI probe with a z-axis gradient system. The acquisition parameters were the same as the D1A and D2A experiments, which are described below. The SSS was sent to NIST-IBBR in Rockville, MD, USA for distribution to all partners.

### Production of the unlabeled NIST-Fab

The test protein for the NMR inter-laboratory study was the Fab domain that was produced enzymatically from the NISTmAb PS #8670, which was formulated at 100 mg/mL in 25 mM L-histidine, pH 6.0.<sup>33</sup> To generate a sufficient quantity of the unlabeled NIST-Fab protein for the study, the NISTmAb at 8 mg/mL was digested using immobilized papain cross-linked on agarose beaded support (ThermoFisher Scientific, Waltham, MA). Following the cleavage of the NISTmAb into the Fab and Fc domains, the NIST-Fab was purified with a HiTrap rProtein A FF affinity column (GE Healthcare Life Sciences, Pittsburgh, PA). It was subsequently passed through a 100 kDa MWCO Amicon filter (EMD Millipore Corporation, Billerica, MA) to remove high molecular weight impurities, followed by a 30 kDa MWCO Amicon filter (EMD Millipore Corporation, Billerica, MA) to remove low molecular weight contaminants. During the final filtration step, the NIST-Fab was buffer exchanged into 25 mM bis-tris-*d*19, pH 6.0, in 95% H<sub>2</sub>O and 5% D<sub>2</sub>O. The final concentration of the NIST-Fab was adjusted with buffer to 429 μM, which was measured on a NanoDrop 2000

spectrophotometer (ThermoFisher Scientific, Waltham, MA) using a theoretical extinction coefficient of 69.95 mM<sup>-1</sup>cm<sup>-1</sup>.

### Distribution of samples

All 5 mm NMR microtubes matched to the NMR spectrometer vendor type (*i.e.*, Agilent or Bruker BioSpin) found in each of the partnering laboratories were purchased from Shigemi, Inc (Allison Park, PA). The NMR tubes were pre-loaded with the SSS or the NIST-Fab samples (275 μL each) at NIST with an air bubble to allow for water expansion in the event that the samples froze during shipment. All samples were shipped cold. Upon receipt, each laboratory was instructed to store the sample at 4 °C until NMR time could be scheduled. The air bubble between the plunger and sample was removed by each collaborating laboratory before any measurements were performed.

### Instrumentation

A total of 39 magnet systems were employed in the inter-laboratory study. Field strengths ranged from 500 MHz to 900 MHz magnets manufactured by Bruker BioSpin (Billerica, MA) or Varian/Agilent (Santa Clara, CA) equipped with cold or standard room temperature probes (Table 2 and Table S4). To reduce the likelihood of traceability of data to a collaborating laboratory, the full hardware list was provided to NIST by a third party contractor, National Association of Proficiency Testing (NAPT, Edina, MN), in a randomized fashion.

### Blinding of data

All data was submitted directly to NAPT for data anonymization by each laboratory. NAPT converted all vendor-specific raw data into NMRPipe<sup>34</sup> format using version (V)8.9 and assigned an anonymous code. The code consisted of a 4-digit institutional identifier followed by a 3-digit experiment number (*e.g.*, 1247–001). When coupled with experimental type (see Summary of experiments section, below), each experiment received a final 10-digit code (*e.g.*, D2A-1247–001). All anonymized spectra were then submitted to NIST. Institutions who submitted more than one data package received multiple institutional identifiers.

### Temperature calibration

The temperature of each magnet was calibrated using perdeuterated methanol in a 5 mm NMR sealed tube (Sigma Aldrich, Inc., St. Louis, MO). A total of three 1D <sup>1</sup>H experiments were recorded at 310 K. The normalized temperature was calculated using the following equation:

$$T = -16.7467 \times (\Delta\delta)^2 - 52.5130 \times \Delta\delta + 419.1381$$

where Δδ is the chemical shift difference in ppm between the methyl and hydroxyl resonances, and T is the absolute temperature of the sample in Kelvin. The temperature of the probe was adjusted so that it was 310 K ± 0.1 K,

**Table 2.** Summary of 39 NMR spectrometers.

<sup>1</sup> H Frequency	Number of Magnets
500 MHz	3
600 MHz	16
700 MHz	6
750 MHz	2
800 MHz	6
850 MHz	3
900 MHz	3



corresponding to a chemical shift difference of 1.428 ppm. The calibration was additionally performed by each institution that collected spectra at 288 K, 298 K, 318 K, and 323 K, corresponding respectively to chemical shift differences of 1.640 ppm, 1.545 ppm, 1.347 ppm, and 1.295 ppm. All temperatures are given in degrees Celsius elsewhere in this report.

### Summary of experiments

Each partnering laboratory conducted a series of required  $^1\text{H}$ ,  $^{15}\text{N}$  and  $^1\text{H}$ ,  $^{13}\text{C}$  gHSQC experiments<sup>35</sup> at 37 °C with uniform and non-uniform sampling and could additionally perform optional experiments to further explore methodological space. All experiments are summarized in Table 1, and detailed acquisition parameters are given in Tables S5 to S9. The choice of all unspecified experimental parameters (*e.g.*, field strength of pulses, details of decoupling, recycling delay) were left to the operators of the partnering laboratories. For a more detailed list of performed experiments, see Table S1. In general, the required experimental protocol probed uniform sampling and non-uniform sampling in both a field independent (experiments D2A and D2B) and field dependent (experiments D1A, D2C, D2D, D2E, D3A, and D3B) manner. Optional experiments explored different pulse sequences such as the SOFAST-HMQC (sfHMQC, experiments E1C and E2C)<sup>26</sup> and phase sensitive HSQC (pHSQC, experiment E2B).<sup>36</sup> Other optional measurements included the collection of spectra at 15 °C, 25 °C, 45 °C, and 50 °C (experiments E1B and E2A). Many laboratories also generated custom NUS schedules (experiments E1A and E2N).

### Generation of NUS schedules

The NIST-supplied NUS schedules were generated using the Poisson-gap algorithm<sup>31</sup> by Prof. Gerhard Wagner's research group at the Harvard Medical School in Boston, MA. These NUS schedules were then sent to NIST. Custom schedules on Bruker magnet systems were generated with the default schedule in the TopSpin 3 software, which uses a multi-dimensional probability density function. Laboratory 1894 used the Kupče option of the vNMRJ 3.2 software, which used an algorithm for random sampling with no T2 weighting. Laboratory 4233 also used the SineBurst and SineGap algorithms<sup>37</sup> to generate custom NUS schedules.

### Spectral processing

All spectra were processed with NMRPipe V8.9<sup>34</sup> using a 54° ( $^1\text{H}$ ) and 90° ( $^{13}\text{C}$  and  $^{15}\text{N}$ ) shifted sine squared window function and zero-filled to quadruple the points in both dimensions before Fourier transform (FT). For uniformly sampled spectra in the indirect dimension, forward-backwards linear prediction to double the number of points was applied prior to zero-filling and FT. For NUS spectra, data were reconstructed using iterative soft thresholding within NMRPipe.<sup>38</sup> All spectra were visualized in NMRFAM-Sparky V1.4.<sup>39</sup> To calibrate the spectra, separate SSS and NIST-Fab samples were prepared with the standard chemical shift reference molecule, 4,4-dimethyl-4-silapentane-

1-sulfonic acid (DSS).<sup>40</sup> Three sequential experiments, 1D  $^1\text{H}$ , 2D  $^{13}\text{C}$  or  $^{15}\text{N}$ , and 1D  $^1\text{H}$ , were collected on these doped samples. The  $^1\text{H}$  methyl signal of DSS was set to 0.000 ppm and the  $^{13}\text{C}$  and  $^{15}\text{N}$  chemical shift references set based on conversion factors determined from their gyromagnetic ratios. Alignment of spectra was performed on an arbitrarily numbered isolated cross peak that had negligible shifting due to temperature. For  $^1\text{H}$ ,  $^{15}\text{N}$  data, the cross peak located at  $\delta_{\text{H}}$  7.546 ppm and  $\delta_{\text{N}}$  118.978 ppm (cross peak #68, Figure S1) was used for spectral alignment; for  $^1\text{H}$ ,  $^{13}\text{C}$  spectra, the cross peak located at  $\delta_{\text{H}}$  0.513 ppm and  $\delta_{\text{C}}$  17.494 ppm was used (cross peak #29, Figure S2). Arbitrarily numbered peaks lists were created by using the peak-picking feature within NMRFAM-Sparky on a representative 500 MHz spectrum. This peak list was then copied to all other spectra for both the SSS and the NIST-Fab at all temperatures, and each peak was centered using the peak-centering command. For defined peaks that were doublets in the  $^{13}\text{C}$  dimension likely due to higher incorporation of two  $^{13}\text{C}$  nuclei at adjacent positions in the SSS, the center of the peak was determined using a 1D trace and taking the chemical shift difference between each peak of the doublet and dividing by two. This multiplet spectral signature is an artifact of fractionally enriching the SSS with 20%  $^{13}\text{C}$ <sup>41</sup> and will not be an issue for spectra of unlabeled biopharmaceuticals collected at natural isotopic abundance. A total of 187 and 95 cross peaks were chosen for  $^1\text{H}$ ,  $^{15}\text{N}$  and  $^1\text{H}$ ,  $^{13}\text{C}$  spectra, respectively, for in-depth analysis of peak position. Poor average signal-to-noise ( $S/N < 10:1$ ) or otherwise poor resolution precluded the ability to create peak lists for a number of spectra (Table S10, Figures S14 and S15). Of the 375  $^1\text{H}$ ,  $^{13}\text{C}$  HSQCs, 354 were included in the spectral analysis in this report. For  $^1\text{H}$ ,  $^{15}\text{N}$  HSQCs, only spectra of the SSS (41 of 76) were included in this report due to the difficulty of reliably tracking peak movement at different temperatures, so only spectra recorded at 37 °C were included in the CCSD analyses.

### Statistical analysis

All peak lists generated from the spectra were analyzed using CCSD or with PCA. True outliers in this study are those spectra that were excluded from the analyses in this report (Table S10). In general, these outliers were the result of hardware problems or failure to achieve the suggested average  $S/N$  of 10:1 (see the Spectral processing sub-section for more details).

### Combined chemical shift deviation

CCSDs were computed for  $^1\text{H}$ ,  $^{15}\text{N}$  and  $^1\text{H}$ ,  $^{13}\text{C}$  spectra, separately in Microsoft Excel (Redmond, WA), according to the following equation:

$$\text{CCSD} = \sqrt{0.5 * [(\delta_{\text{H}} - \delta_{\text{H,ref}})^2 + (\alpha\delta_{\text{X}} - \alpha\delta_{\text{X,ref}})^2]}$$

where  $\delta_{\text{H}}$  and  $\delta_{\text{X}}$  are the  $^1\text{H}$  and  $^{15}\text{N}$  or  $^{13}\text{C}$  chemical shifts, respectively, of a given cross peak;  $\delta_{\text{H,ref}}$  and  $\delta_{\text{X,ref}}$  are the  $^1\text{H}$  and  $^{15}\text{N}$  or  $^{13}\text{C}$  reference chemical shifts, respectively for

the same cross peak; and the frequency weighting factor,  $\alpha$ , is equal to 0.1 or 0.251 for  $^{15}\text{N}$  and  $^{13}\text{C}$ , respectively.<sup>15,28</sup> Reference average peak lists were generated from D1A  $^1\text{H}$ ,  $^{15}\text{N}$  spectra and D2A and D2C  $^1\text{H}$ ,  $^{13}\text{C}$  spectra, respectively (Tables S11 and S12). An average CCSD value was then computed for each acquired spectrum. Error bars were determined using the standard error of the mean (SEM) with 95% confidence intervals according to the equation:

$$\text{SEM} = \mu \pm 1.96 * \sigma / \sqrt{n}$$

where  $\mu$  is the average CCSD,  $\sigma$  is the sample standard deviation, and  $n$  is the number of spectra.

### Principal component analysis

Principal component analysis (PCA) was applied using the single value decomposition algorithm from the Statistics and Machine Learning Toolbox<sup>TM</sup> in MATLAB (Mathworks, Inc, Natick, MA). To prepare the peak lists for PCA, unreferenced  $^1\text{H}$ ,  $^{13}\text{C}$  chemical shifts were weighted in a manner similar to CCSD.

$$\delta_{\text{weighted}} = \sqrt{0.5 * [(\delta_{\text{H}})^2 + (\alpha\delta_{\text{C}})^2]}$$

To mean-center the weighted chemical shift values for each peak, the D2A and D2C spectra were chosen as the 'benchmark' spectra because they were acquired with the conventional uniformly sampled gHSQC experiment. The weighted chemical shifts for all D2A and D2C peak lists were averaged together for each peak to generate an average weighted peak list. These values were then subtracted from the weighted peak list of each individual spectrum. All spectra were then combined into a matrix of 354 spectra by 95 mean-centered peak positions for input into the PCA algorithm. Appropriate grouping of PCA results, where applicable (see main text), was determined manually by sample type and temperature or by chemometric clustering methods, such as  $k$ -medoids, min-max group pair, or UPGMA.<sup>42,43</sup> Confidence ellipsoids of 95% and 99% using chi-square probabilities were then plotted for each cluster.

### Clustering algorithms

Three clustering algorithms were employed: the  $k$ -medoids algorithm, min-max group pair method, and UPGMA. For the  $k$ -medoids method, the algorithm seeks to partition spectra into  $k$  clusters of minimal intra-cluster distance. To find these clusters, a heuristic was employed wherein initial clusters were chosen by assigning each spectra to its closest cluster center. The initial cluster centers were taken to be the  $k$  elements that maximized the sum of pair-wise dissimilarities. Having chosen  $k$  initial clusters, a heuristic was applied to find the clustering assignment of minimal intra-cluster distance. This was done by iteratively swapping each point that was a cluster center with each point that was not a cluster center; if the resulting configuration decreased intra-cluster distance, then the configuration was updated to reflect the swap. If not, the swap was reversed. This swapping procedure was iteratively applied to all points until the clustering configuration no longer changed and is analogous to the SWAP step in the PAM heuristic.<sup>44</sup>

While the  $k$ -medoids algorithm is a partitioning algorithm, the min-max group pairing algorithm and UPGMA algorithms are

hierarchical in nature. In hierarchical clustering algorithms, each element is initially in a singleton cluster. If there are  $n$  elements to be clustered, there are initially  $n$  clusters. Clusters are iteratively merged until all elements are in a single cluster. The UPGMA algorithm and the min-max group pair algorithm differ in the manner in which clusters are merged: the former merges the two closest clusters at each iteration, while the latter maximizes the ratio of inter-cluster distance to intra-cluster distance. It should be noted that the min-max group pair algorithm is a novel hierarchical clustering algorithm and has been employed for the first time in the present work.

### Public data repository

All blinded raw data in NMRPipe format, including NUS schedules and processing scripts, are available at the following URL: [www.ibbr.umd.edu/groups/nistmab-nmr](http://www.ibbr.umd.edu/groups/nistmab-nmr)

### Disclaimers

Certain commercial equipment, instruments, and materials are identified here in order to specify the experimental procedure. Such identification does not imply recommendation or endorsement by the National Institute of Standards and Technology, nor does it imply that the material or equipment identified is necessarily the best available for the purpose. This article reflects the views of the author and should not be construed to represent the U.S. Food and Drug Administration's views or policies.

### Abbreviations

2D	two-dimensional
CCSD	combined chemical shift deviation
CD	circular dichroism
FT-IR	Fourier transform infrared spectroscopy
gHSQC	gradient-selected heteronuclear single quantum coherence spectroscopy
HOS	higher order structure
mAb	monoclonal antibody
NIST	National Institute of Standards and Technology
NMR	nuclear magnetic resonance
NUS	non-uniform sampling
pHSQC	phase sensitive heteronuclear single quantum coherence spectroscopy
PAGE	polyacrylamide gel electrophoresis
PCA	principal component analysis
PS	primary sample
QA	quality attribute
RM	reference material
SEM	standard error of the mean
SSS	system suitability sample
SOFAST-HMQC	selective optimized flip angle short transient heteronuclear multiple quantum coherence spectroscopy
UPGMA	Unweighted Pair Group Method with Arithmetic Mean

### Acknowledgments

Biogen gives special thanks to the NMR facility and Jean-Christophe Hus for supporting the Biomolecular NMR instrumentation and technical support. We acknowledge Gerhard Wagner, Sven Hyberts, and Haribabu Arthanari for discussions related to experimental design of the NUS component of this project. We also acknowledge their generation of the actual NUS schedules

used in the study. Leibniz-Forschungsinstitut für Molekulare Pharmakologie (FMP) acknowledges Monika Beerbaum. NRC Canada thanks Lynne LeSauter, Director of Downstream Processing and Analytics, for her interest and encouragement. Yung-Hsiang Kao, Associate Director of Protein Analytical Chemistry at Genentech is acknowledged.

## Competing Financial Interests

None Declared.

## Disclosure statement

No potential conflict of interest was reported by the authors.

## Funding

NIST acknowledges the support by NIST Biomanufacturing Program and NIST and W.M. Keck Foundation for support of biomolecular NMR instrumentation. The work at Stockholm University was supported by a grant from the Knut and Alice Wallenberg Foundation. The Brazilian Center for Research in Energy and Materials acknowledge the support by the Brazilian Ministry of Science, Technology, Innovation and Communication (MCTIC). A portion of the research was performed using NMR instrumentation at EMSL, a DOE Office of Science User Facility sponsored by the Office of Biological and Environmental Research and located at Pacific Northwest National Laboratory. This work at Health Canada was supported by Government of Canada. The work at NRC Canada was supported by the NRC Biologics and Biomanufacturing Program and by the Department of Downstream Processing and Analytics (for Protein NMR instrumentation), for which this paper is assigned the NRCC Publication No. NRC\_HHT\_53378. The work at the University of Queensland was supported by the Australian Research Council and The National Health and Medical Research Council as well as the University of Queensland. BNSP (Biomolecular NMR Spectroscopy Platform) ETH Zürich, is acknowledged for providing equipment and infrastructure. The NMR facility used for this work is supported by the Office of the Vice President for Research at the Medical University of South Carolina. The NMR maintenance was supported in part by the Nanotechnology Platform Program (Molecule and Material Synthesis) and by the grants (JP25102001, JP25102008, JP15K21708 and JP15H02491 to K.K.; JP17H05893 and 18K14892 to S.Y.) from the Ministry of Education, Culture, Sports, Science and Technology (MEXT) of Japan.

## ORCID

Luke W. Arbogast  <http://orcid.org/0000-0001-6871-450X>  
 Houman Ghasriani  <http://orcid.org/0000-0002-9646-0006>  
 Yves Aubin  <http://orcid.org/0000-0002-8554-0297>  
 Xinying Jia  <http://orcid.org/0000-0002-2831-4605>  
 Mehdi Mobli  <http://orcid.org/0000-0003-2420-4262>  
 Jonas Stähle  <http://orcid.org/0000-0001-5657-8635>  
 Patrick N. Reardon  <http://orcid.org/0000-0002-6858-0086>  
 John R. Cort  <http://orcid.org/0000-0001-6342-6461>  
 Stuart R. Parnham  <http://orcid.org/0000-0002-8205-5827>  
 Andreas Blomgren  <http://orcid.org/0000-0001-8171-4678>  
 Torgny Rundlöf  <http://orcid.org/0000-0001-9004-7272>  
 Nils Trieloff  <http://orcid.org/0000-0002-3530-9273>  
 Kang Chen  <http://orcid.org/0000-0003-0276-2474>  
 David Keire  <http://orcid.org/0000-0002-7767-7904>  
 Darón I. Freedberg  <http://orcid.org/0000-0003-1991-5174>  
 Janez Plavec  <http://orcid.org/0000-0003-1570-8602>  
 Christina M. Szabo  <http://orcid.org/0000-0003-0403-6337>  
 Carlos A. Amezcua  <http://orcid.org/0000-0003-1644-8689>

## References

1. Statista: The Statistics Portal. Global top 10 companies based on biotech prescription drug revenue in 2017 and 2024. 2018 June [accessed 2018 Oct 5]. <https://www.statista.com/statistics/309460/biotechnology-prescription-drug-revenue-by-top-ten-companies-globally/>.
2. Stone K. Top 10 biologic drugs in the United States: these drugs are changing the way illnesses are treated. 2018 [accessed 2018 Oct 5]. <https://www.thebalance.com/top-biologic-drugs-2663233>.
3. Kaplon H, Reichert JM. Antibodies to watch in 2018. *mAbs*. 2018;10:183–203. doi:10.1080/19420862.2018.1415671.
4. United States Food and Drug Administration. Scientific Considerations in Demonstrating Biosimilarity to a Reference Product: Guidance for Industry. Silver Spring (MD): United States Food and Drug Administration; 2015.
5. Berkowitz SA, Engen JR, Mazzeo JR, Jones GB. Analytical tools for characterizing biopharmaceuticals and the implications for biosimilars. *Nat Rev Drug Discov*. 2012;11:527–540. doi:10.1038/nrd3746.
6. Borisov OV, Schiel JE, Davis D. Trends and drivers for the development of next-generation biotherapeutic characterization tools. In: Schiel JE, Davis DL, Borisov OV, editors. State-of-the-art and emerging technologies for therapeutic monoclonal antibody characterization, vol 3: defining the next generation of analytical and biophysical techniques. Washington (DC): American Chemical Society; 2015. p. 1–16.
7. Weiss WF, Gabrielson JP, Al-Azzam W, Chen G, Davis DL, Das TK, Hayes DB, Houde D, Singh SK. Technical decision making with higher order structure data: perspectives on higher order structure characterization from the biopharmaceutical industry. *J Pharm Sci*. 2016;105:3465–3470. doi:10.1016/j.xphs.2016.09.003.
8. Fisher AC, Lee SL, Harris DP, Buhse L, Kozlowski S, Yu L, Kopcha M, Woodcock J. Advancing pharmaceutical quality: an overview of science and research in the U.S. FDA's Office of Pharmaceutical Quality. *Int J Pharm*. 2016;515:390–402. doi:10.1016/j.ijpharm.2016.10.038.
9. Gabrielson JP, Weiss WF. Technical decision-making with higher order structure data: starting a new dialogue. *J Pharm Sci*. 2015;104:1240–1245. doi:10.1002/jps.24393.
10. Aubin Y, Gingras G, Sauve S. Assessment of the three-dimensional structure of recombinant protein therapeutics by NMR fingerprinting: demonstration on recombinant human granulocyte macrophage-colony stimulation factor. *Anal Chem*. 2008;80:2623–2627. doi:10.1021/ac7026222.
11. Japelj B, Ilc G, Marusic J, Sencar J, Kuzman D, Plavec J. Biosimilar structural comparability assessment by NMR: from small proteins to monoclonal antibodies. *Sci Rep*. 2016;6:32201. doi:10.1038/srep32201.
12. Kiss R, Fizil Á, Szántay C. What NMR can do in the biopharmaceutical industry. *J Pharm Biomed Anal*. 2018;147:367–377. doi:10.1016/j.jpba.2017.07.004.
13. Aubin Y, Freedberg DI, Jones C. Using NMR spectroscopy to obtain the higher order structure of biopharmaceutical products: simple methods can characterize polysaccharide vaccines and recombinant cytokines at high resolution. *Biopharm Int*. 2010; S28+.
14. Arbogast LW, Brinson RG, Marino JP. Application of natural isotopic abundance (<sup>1</sup>H-(<sup>13</sup>C)- and (<sup>1</sup>H-(<sup>15</sup>N)-correlated two-dimensional NMR for evaluation of the structure of protein therapeutics. *Methods Enzymol*. 2016;566:3–34. doi:10.1016/bb.mie.2015.09.037.
15. Ghasriani H, Hodgson DJ, Brinson RG, McEwen I, Buhse LF, Kozlowski S, Marino JP, Aubin Y, Keire DA. Precision and robustness of 2D-NMR for structure assessment of filgrastim biosimilars. *Nat Biotechnol*. 2016;34:139–141. doi:10.1038/nbt.3474.
16. Aubin Y, Hodgson DJ, Thach WB, Gingras G, Sauve S. Monitoring effects of excipients, formulation parameters and



- mutations on the high order structure of filgrastim by NMR. *Pharma Res.* **2015**;32:3365–3375. doi:10.1007/s11095-015-1713-3.
17. Singh SM, Bandi S, Jones DNM, Mallela KMG. Effect of polysorbate 20 and polysorbate 80 on the higher-order structure of a monoclonal antibody and its fab and fc fragments probed using 2d nuclear magnetic resonance spectroscopy. *J Pharm Sci.* **2017**;106:3486–3498. doi:10.1016/j.xphs.2017.08.011.
  18. United States Food and Drug Administration. Clinical Pharmacology Data to Support Demonstration of Biosimilarity to a Reference Product: Guidance for Industry. United States Food and Drug Administration, Silver Spring (MD): **2016**.
  19. Arbogast LW, Brinson RG, Marino JP. Mapping monoclonal antibody structure by 2D <sup>13</sup>C NMR at natural abundance. *Anal Chem.* **2015**;87:3556–3561. doi:10.1021/ac504804m.
  20. Arbogast LW, Brinson RG, Formolo T, Hoopes JT, Marino JP. 2D (1)H(N), (15)N correlated NMR methods at natural abundance for obtaining structural maps and statistical comparability of monoclonal antibodies. *Pharm Res.* **2016**;33:462–475. doi:10.1007/s11095-015-1802-3.
  21. Hodgson DJ, Ghasriani H, Aubin Y. Assessment of the higher order structure of Humira(R), Remicade(R), Avastin(R), Rituxan(R), Herceptin(R), and Enbrel(R) by 2D-NMR fingerprinting. *J Pharm Biomed Anal.* **2019**;163:144–152. doi:10.1016/j.jpba.2018.09.056.
  22. Schiel JE, Mire-Sluis, A, David D. Monoclonal Antibody Therapeutics: The Need for Biopharmaceutical Reference Materials. In: Schiel JE, Davis DL, Borisov OV, editors. State-of-the-Art and Emerging Technologies for Therapeutic Monoclonal Antibody Characterization Volume 1. Monoclonal Antibody Therapeutics: Structure, Function, and Regulatory Space. Washington (DC): American Chemical Society; 2014. p. 1-34.
  23. Schiel JE, Turner A. The NISTmAb Reference Material 8671 life-cycle management and quality plan. *Anal Bioanal Chem.* **2018**;410:2067–2078. doi:10.1007/s00216-017-0844-2.
  24. Schiel JE, Turner A, Mouchahoir T, Yandrowski K, Telikepalli S, King J, DeRose P, Ripple D, Phinney K. The NISTmAb Reference Material 8671 value assignment, homogeneity, and stability. *Anal Bioanal Chem.* **2018**;410:2127–2139. doi:10.1007/s00216-017-0800-1.
  25. Arbogast LW, Delaglio F, Schiel JE, Marino JP. Multivariate analysis of two-dimensional <sup>1</sup>H, <sup>13</sup>C methyl NMR spectra of monoclonal antibody therapeutics to facilitate assessment of higher order structure. *Anal Chem.* **2017**;89:11839–11845. doi:10.1021/acs.analchem.7b03571.
  26. Schanda P, Kupce E, Brutscher B. SOFAST-HMQC experiments for recording two-dimensional heteronuclear correlation spectra of proteins within a few seconds. *J Biomol NMR.* **2005**;33:199–211. doi:10.1007/s10858-005-4425-x.
  27. Mobli M, Hoch JC. Nonuniform sampling and non-Fourier signal processing methods in multidimensional NMR. *Prog Nucl Magn Reson Spectrosc.* **2014**;83:21–41. doi:10.1016/j.pnmrs.2014.09.002.
  28. Williamson MP. Using chemical shift perturbation to characterise ligand binding. *Prog Nucl Magn Reson Spectrosc.* **2013**;73:1–16. doi:10.1016/j.pnmrs.2013.02.001.
  29. European Medicines Agency. ICH Q5E Biotechnological/biological products subject to changes in their manufacturing process: comparability of biotechnological/biological products. London, UK: **2005**, CPMP/ICH/5721/03, step 5.
  30. United States Food and Drug Administration. Considerations in Demonstrating Interchangeability With a Reference Product: Draft Guidance for Industry. Silver Spring (MD): United States Food and Drug Administration; **2017**.
  31. Hyberts SG, Takeuchi K, Wagner G. Poisson-gap sampling and forward maximum entropy reconstruction for enhancing the resolution and sensitivity of protein NMR data. *J Am Chem Soc.* **2010**;132:2145–2147. doi:10.1021/ja908004w.
  32. Schiel JE, Davis DL, Borisov, OV. State-of-the-art and emerging technologies for therapeutic monoclonal antibody characterization volume 2. biopharmaceutical characterization: the NISTmAb case study. Washington (DC): American Chemical Society; **2015**;1201.
  33. Schiel JE, Davis DL, Borisov, OV. State-of-the-art and emerging technologies for therapeutic monoclonal antibody characterization volume 1. monoclonal antibody therapeutics: structure, function, and regulatory space. Washington (DC): American Chemical Society; **2014**;1176.
  34. Delaglio F, Grzesiek S, Vuister GW, Zhu G, Pfeifer J, Bax A. NMRPipe: a multidimensional spectral processing system based on UNIX pipes. *J Biomol NMR.* **1995**;6:277–293.
  35. Grzesiek S, Bax A. The importance of not saturating H<sub>2</sub>O in protein NMR. Application to sensitivity enhancement and NOE measurements. *J Am Chem Soc.* **1993**;115:12593–12594. doi:10.1021/ja00079a052.
  36. Sklenár V, Piotta M, Leppik R, Saudek V. Gradient-tailored water suppression for <sup>1</sup>H - <sup>15</sup>N HSQC experiments optimized to retain full sensitivity. *J Magn Reson A.* **1993**;102:241–245. doi:10.1006/jmra.1993.1098.
  37. Worley B, Powers R. Deterministic multidimensional nonuniform gap sampling. *J Magn Reson.* **2015**;261:19–26. doi:10.1016/j.jmr.2015.09.016.
  38. Hyberts SG, Milbradt AG, Wagner AB, Arthanari H, Wagner G. Application of iterative soft thresholding for fast reconstruction of NMR data non-uniformly sampled with multidimensional Poisson Gap scheduling. *J Biomol NMR.* **2012**;52:315–327. doi:10.1007/s10858-012-9611-z.
  39. Lee W, Tonelli M, Markley JL. NMRFAM-SPARKY: enhanced software for biomolecular NMR spectroscopy. *Bioinformatics.* **2015**;31:1325–1327. doi:10.1093/bioinformatics/btu830.
  40. Markley JL, Bax A, Arata Y, Hilbers CW, Kaptein R, Sykes BD, Wright PE, Wüthrich K. Recommendations for the presentation of NMR structures of proteins and nucleic acids. IUPAC-IUBMB-IUPAB inter-union task group on the standardization of data bases of protein and nucleic acid structures determined by NMR spectroscopy. *J Biomol NMR.* **1998**;12:1–23.
  41. Wenrich BR, Sonstrom RE, Gupta RA, Rovnyak D. Enhanced biosynthetically directed fractional carbon-13 enrichment of proteins for backbone NMR assignments. *Protein Expr Purif.* **2015**;115:1–10. doi:10.1016/j.pep.2015.08.005.
  42. Kaufman L, Rousseeuw PJ. Clustering by means of medoids. In: Diodge Y, editor. Statistical data analysis based on the L<sub>1</sub> Norm and Related Methods. North Holland (MI): University of Michigan; **1987**. p. 464.
  43. Sokal RR. A statistical method for evaluating systematic relationship. *Univ Kans Sci Bull.* **1958**;28:1409–1438.
  44. Kaufman L, Rousseeuw PJ. Finding groups in data: an introduction to cluster analysis. Hoboken (NJ): John Wiley & Sons, Inc; **2005**.



Minerva Access is the Institutional Repository of The University of Melbourne

**Author/s:**

Brinson, RG; Marino, JP; Delaglio, F; Arbogast, LW; Evans, RM; Kearsley, A; Gingras, G; Ghasriani, H; Aubin, Y; Pierens, GK; Jia, X; Mobli, M; Grant, HG; Keizer, DW; Schweimer, K; Stahle, J; Widmalm, G; Zartler, ER; Lawrence, CW; Reardon, PN; Cort, JR; Xu, P; Ni, F; Yanaka, S; Kato, K; Parnham, SR; Tsao, D; Blomgren, A; Rundlof, T; Trieloff, N; Schmieder, P; Ross, A; Skidmore, K; Chen, K; Keire, D; Freedberg, DI; Suter-Stahel, T; Wider, G; Ilc, G; Plavec, J; Bradley, SA; Baldisseri, DM; Sforca, ML; de Mattos Zeri, AC; Wei, JY; Szabo, CM; Amezcua, CA; Jordan, JB; Wikstrom, M

**Title:**

Enabling adoption of 2D-NMR for the higher order structure assessment of monoclonal antibody therapeutics

**Date:**

2019-01-02

**Citation:**

Brinson, R. G., Marino, J. P., Delaglio, F., Arbogast, L. W., Evans, R. M., Kearsley, A., Gingras, G., Ghasriani, H., Aubin, Y., Pierens, G. K., Jia, X., Mobli, M., Grant, H. G., Keizer, D. W., Schweimer, K., Stahle, J., Widmalm, G., Zartler, E. R., Lawrence, C. W. ,... Wikstrom, M. (2019). Enabling adoption of 2D-NMR for the higher order structure assessment of monoclonal antibody therapeutics. *mAbs*, 11 (1), pp.94-105.  
<https://doi.org/10.1080/19420862.2018.1544454>.

**Persistent Link:**

<http://hdl.handle.net/11343/250348>

**File Description:**

published version

**License:**

CC BY-NC-ND